Robot-Assisted Disassembly Sequence Planning with Real-Time Human Motion Prediction

Meng-Lun Lee[1], Wansong Liu[1], Sara Behdad[2], Xiao Liang[3,*] and Minghui Zheng[1,*]

***Abstract*—This paper presents a disassembly task planning algorithm considering human-robot collaboration (HRC) and human behavior prediction (HBP). Unlike assembly procedures, the disassembly of end-of-life (EOL) products has been a labor-intensive process with uncertainties difficult to cope with. Meanwhile, it is usually challenging to obtain an optimal sequence efficiently without excessive computational cost. Also, the conventional human-centered task planning, in which the robot has to halt frequently due to unsafe interruptions by human motions, may decrease the efficiency of the disassembly process. In this paper, a sequence planner is proposed to assign tasks in real-time between a human operator and a robot to overcome the aforementioned challenges. The cost function includes the effort of the human and the robot in terms of both movement distance and time spent on the tasks. The constraints include the disassembly rules and safety of human operation. The optimal sequence is generated by solving an optimization problem in a receding-horizon way. In particular, at each step, the proposed disassembly sequence planner locates the workers (a human operator and a robot) and the to-be-disassembled components, predicts human movement for the next several steps, and obtains the optimal disassembly sequence for the next several steps following disassembly rules and safety constraints. Experiments have been extensively conducted on the disassembly of a wooden toybox and a used hard disk drive (HDD) to validate the proposed disassembly sequence planner. The planner has successfully generated the disassembly sequence in a human-robot collaboration setting explicitly considering real-time human motion prediction and assigned the human operator and the robot to collaboratively complete disassembly tasks without violating disassembly rules and safety constraints.**

***Index Terms*—Human-Robot Collaboration, Disassembly Sequence Planning, Human Behavior Prediction, Receding Horizon.**

I. Introduction

Environmentally conscious manufacturing (ECM) has drawn attention due to the increased legislation of recycling end-of-life (EOL) products, which is usually achieved through manual disassembly. The disassembly process has been traditionally time-consuming and labor-intensive [1]. In order to improve the process, human-robot collaboration (HRC) is developed to exploit the complementary advantages of both humans and robots, as humans have experience and flexibility to react to uncertainties in assignments, while robots could offer accuracy and efficiency in assigned tasks and the capability of handling unsafe tasks that may cause human injuries [2].

Disassembly sequence planning plays a major role in achieving efficiency and cost-effectiveness in disassembly process. Disassembly sequences consist of actions of removing components one after another [3]. The action of an EOL product disassembly is usually determined from an engineering point of view. For example, desktops and monitors are usually dismantled into sub-assemblies [4] of recyclable mechanical and electrical parts. Disassembly sequence planning is known to be an NP-hard combinatorial optimization problem [4]–[7]; as a large number of feasible disassembly sequences may exist for a set of EOL products and the number grows quickly as the complexity of the product increases. Since it is difficult to obtain the optimal disassembly sequence considering various disassembly constraints, such as disassembly rules, disassembly cost and human safety, it is needed to explore a systematic and efficient approach to finding an optimal sequence.

It is worth noting that the disassembly sequence has its unique characteristics and it should not be stereotyped as the reverse of the assembly [8]. An assembly line is typically conducted in a work-cell format with multiple workstations, customized fixtures [9] and robots programmed for repetitive tasks [10], [11]. Also, the assembly process does not possess many attributes that can be found in the disassembly line. For example, the same component with different conditions, multiple workers available for the same disassembly task, and even variants among different brands in the same disassembly line. In addition, the human worker's position after performing a task cannot be determined at the beginning of the disassembly sequence, causing the difficulty of obtaining the optimal disassembly sequence. Evidently, the decisions of assigning workers to the disassembly tasks would be more complex with both the human operator and the robot being available [12]. Thus, the disassembly process is more challenging for several reasons: (a) distinctive EOL products may be loaded to the same disassembly line with arbitrary orientations instead of building separate disassembly lines; (b) it is common to disassemble highly valuable components without completely dismantling the whole set of EOL products [4]; (c) the to-be-disassembled products may contain components with hazardous substances that need to be handled cautiously. There are several methods to represent feasible disassembly sequences including incidence matrix [13], AND/OR graphs [14], directed graphs [15], and precedence relationships [16]. And several optimization methods have been developed to find the optimal disassembly sequence among feasible sequences [17], [18]. However, existing methods are elaborated based on the assumption of the

[1]Meng-Lun Lee, Wansong Liu, and Minghui Zheng are with the Department of Mechanical and Aerospace Engineering, University at Buffalo, Buffalo, NY 14260, USA. E-mails: {menglunl, wansongl, mhzheng}@buffalo.edu.

[2]Sara Behdad is with the Department of Environmental Engineering Sciences, University of Florida, Gainesville, FL 32611, USA. E-mail: sarabehdad@ufl.edu.

[3]Xiao Liang is with the Department of Civil, Structural and Environmental Engineering, University at Buffalo, Buffalo, NY 14260, USA. E-mail: liangx@buffalo.edu.

*Corresponding authors.

disassembly process usually being conducted manually.

Collaborative manufacturing systems have been studied in various assembly line applications. The desire of improving manufacturing productivity and flexibility is a crucial motivation for research in HRC assembly systems [19]. For instance, in [20], an augmented reality (AR) system is used to support the human operator in automotive assembly line with HRC. The AR system is used to visualize necessary information from the assembly line without interrupting the human operator. In [21], a framework for an electronics assembly system considering HRC is presented consisting of product characteristics and safety considerations. In [22], a dynamic task allocation and classification for mechanical assemblies is proposed to determine whether the assembly activities can be performed by the human and/or the robot. In [23], a simulation-based multi-objective optimization method is presented for assigning the assembly tasks to both the human operator and the robot. In [24], the complexity of the assembly processes is evaluated, which includes geometrical and physical properties of the assembly components alongside the safety issues in the assembly tasks. In [25], a measured cycle time is used to evaluate the skill index of a human operator, which helps effectively predict the assembly process and balances the workloads of the human operator and the robot. Also, a mixed-integer linear programming (MILP) model integrated with bee algorithm (BA) and artificial bee colony (ABC) algorithms is presented in [26] to solve a large-scale assembly line balancing problem with HRC. Most assembly frameworks aim to define the task assignments appropriately in a human-robot collaborative assembly line. Still, unlike the disassembly line, the uncertainty regarding the quality of the components is not taken into account.

A systematic framework for the implementation of HRC disassembly was presented for sustainable manufacturing [27]. Deep learning techniques, such as incremental learning, deep reinforcement learning, and transfer learning, have been proposed to tackle with HRC disassembly problem [27]. Although HRC has been widely applied in the industry, it is still difficult to perceive the status of human intention, robot motion and disassembly products. In [28], with HRC disassembly, the performance of human operators and robots is assessed in the aspects of quality, cost, time, and safety, but the uncertainties in the movement of the human operator are not included. [29] gives a solution to the HRC disassembly line balancing problem, but the potentially hazardous condition of the disassembly parts is not considered. In addition, an HRC disassembly sequence planning is carried out through a hybrid resource assignment and scheduling problem using MILP [30], and an HRC disassembly cell based on touch-sensing and position control [31] is conducted to distribute the disassembly tasks. Our previous work [32] introduces a parallel disassembly sequence planning considering human safety using MILP. However, those studies do not particularly focus on the human motion prediction and do not consider the human worker's position associated with the unfinished disassembly tasks.

In this paper, we introduce HRC to the disassembly process and propose a real-time sequence planning algorithm that can distribute tasks between human operators and robots. There are multiple factors to be considered. The first consideration lies in the human movement that is changing in real-time. A shared task needs robots and human workers to share the working environment and collaborate closely, so HRC should take into account human movement intention and possible future movements. Researchers have proposed different human motion prediction methods that focus on either the trajectory generation level [33]–[35] or the task planning level. For example, depth images are used in [36] to train a conditional variational auto-encoder that has the ability to predict human action. In [37], human poses are used as inputs for training a recurrent neural network to predict time-dependent human motions. In [38], the multiple-predictor system is employed to predict human motion over both short- and long-term horizons. The short-term prediction helps collision avoidance, while the long-term one enables efficient goal-reaching. In [39], human motion at each time step is encoded as a multivariate Gaussian distribution and predicted as the reaching target by Bayesian classification, which is also integrated in the prediction to adjust the robots next action. In [40], human adaptation to the partners motion is captured during an assembly task to learn a cost function, which is used as the input of stochastic trajectory optimizer for motion planning to predict human's reaching motion to a goal region in the task-space. In [41], a support vector machine based on human gaze patterns is trained to predict human intention that enables robots to respond and complete tasks faster. In [42], the hidden Markov model is applied to generate a motion transition probability matrix, where predicted human intention is used to assist in robot task sequence planning in an assembly task. In [43], assembly tasks are modeled as a Bayes network with optimal robot actions to minimize the time cost of human motion prediction.

The second consideration is how to quantify the "disassembly cost" of the human operator and the robot. In this paper, the distance from one disassembly task to another [44] and the working time at each disassembly task [45] are studied to quantify the disassembly cost. For instance, a pick and place action performed by a robot or by a human operator could take different lengths of trajectories and time. Additionally, the geometric complexity of the to-be-disassembled components should be considered, since both the complexity of task execution and the traveling time between each disassembly task may not remain constant if the disassembly task features a diverse set of orientations and unsafe conditions for human operation. Moreover, the human operator may be prohibited from either an unsafe work environment [16] or hazardous materials. Thus, a decision-making framework should be developed for distributing disassembly tasks between robots and human operators following safety constraints.

The third consideration lies in multiple possible starting tasks and disassembly rules. Multiple hierarchical graph models [46] may be used to represent the precedence relation of disassembly tasks. About disassembly rules, take Fig. 1b for example, tasks v_1, v_2 and v_3 must be complete ahead of task v_4; meanwhile, task v_4 must be planned prior to tasks v_5, v_6 and v_7. The task v_4 is also known as the "common task" [45], while v_1, v_2 and v_3 are "parallel tasks" [45], so are v_5, v_6 and v_7. Either v_1, v_2 or v_3 can be the starting task, and the last task can be v_5, v_6 or v_7.

The fourth consideration lies in the computational cost for real-time planning. An EOL product may consist of a significant number of components, leading to a high computational cost. For example, if there is an HRC disassembly with T tasks which

are all parallel tasks, the number of feasible sequences would be $2^T \times T!$, where 2^T is produced by the collaboration of one robot and one human operator, and $T!$ is defined by the number of parallel tasks. To solve the problem with reasonable computational cost, the receding-horizon control (RHC) technique [47] could be adapted. In comparison, if we use the RHC approach with the receding-horizon length t where $t < T$, the number of feasible sequences at each disassembly step would drop to $2^t \times t!$, yielding computational cost reduction.

It is noted that, the above-mentioned considerations are not independent. For example, human behavior during the disassembly process could result in time-varying costs and affect the optimization of disassembly sequence in real-time. After a disassembly task, the human operator may move to a nearby position [48]. This human activity could increase or reduce the disassembly cost. Hence, it is beneficial to incorporate human behavior prediction (HBP) [49] to assure efficiency. Approaches using human activity prediction [50] and user intention prediction [51] have been studied to forecast the human operator's next-step actions. However, these studies are not proposed in the disassembly sequence planning setting.

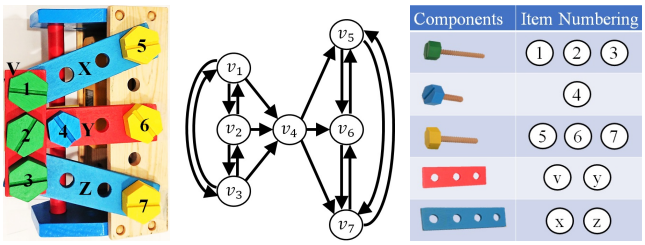

(a) Toybox (b) Directed graph (c) Components

Fig. 1: To-be-disassembled wooden toybox

This paper presents a disassembly task planning algorithm considering HRC and HBP. The sequence planner distributes tasks between the human operator and the robot in real-time. The main contributions of this paper are: (1) the disassembly task sequence planning is conducted as an optimization problem and solved online in a receding-horizon fashion, (2) safety conditions for human operation, positions of the workers and the components to be disassembled, and disassembly rules are considered explicitly, (3) HBP is integrated into the task planner to improve the disassembly efficiency, (4) the cost of disassembly operations with the robot and the human operator is quantified, and (5) the distribution of the disassembly tasks between the human operator and the robot is optimized in a human-robot collaborative setting. The proposed disassembly sequence planning framework is illustrated in Fig. 2 with a wooden toybox as in Fig. 1a. It is noted that this paper is an in-depth extension of our previous conference papers [44], [48], in which the human motion prediction is not considered. To the best of our knowledge, this is the first extensive study on HRC disassembly sequence planning considering the cost, real-time computational efficiency, as well as HBP. Additionally, the study focuses on complete disassembly [52] in the scope of the disassembly of a wooden toybox (see Fig. 1a) and a used hard disk drive (HDD) (see Fig. 12a), and it is possible to adapt the proposed problem formulation to disassembly processes with larger scales.

The rest of the paper is constructed as follows. Section II describes the disassembly scenario and several considerations in the disassembly process. Section III describes the real-time HBP. Section IV presents the proposed sequence planner considering disassembly rules, safety constraints and HBP. Section V introduces the experimental platform and the evaluation of the proposed algorithm. Section VI concludes this paper.

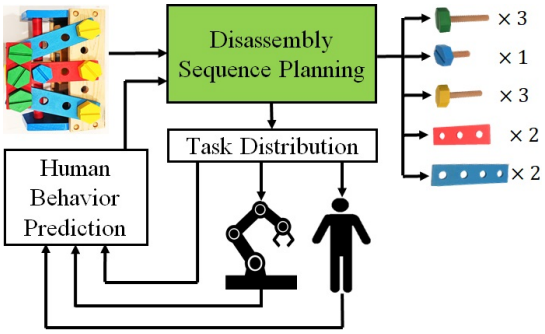

Fig. 2: Proposed framework of disassembly task planning

II. Disassembly Scenario

Before searching for the optimal disassembly sequence, it is crucial to acquire the information of the to-be-disassembled components, including the positions and conditions of the components. If they are not collected correctly, the robot cannot locate the to-be-disassembled components properly and the human operator may be assigned to the unsafe tasks by accident. A wooden toybox (see Fig. 1a) is constructed for demonstration purpose, in which the to-be-disassembled components are Screw 1, 2, ..., 7 and rectangular parts V, X, Y, Z, as shown in Fig. 1c.

1) Disassembly rules: The directed graph model corresponding to the wooden toybox is illustrated in Fig. 1b, in which $v_1, v_2, ..., v_7$ are denoted as the disassembly tasks of Screw 1, 2, ..., 7. We define R_x as the action of "Removing" a component x, where x denotes any of the screws or the rectangular parts. Also, the notation of "$\wedge$" denotes that the tasks on both sides of "$\wedge$" are parallel tasks. And the notation of "$\rightarrow$" indicates that the left-hand side task of "$\rightarrow$" has the higher priority to be disassembled. According to Fig. 1b, the preliminary disassembly rules are (i) $R_1 \wedge R_2 \wedge R_3 \rightarrow R_V$, (ii) $R_V \wedge R_4 \rightarrow R_W$, (iii) $R_V \wedge R_5 \rightarrow R_X$, (iv) $R_W \wedge R_6 \rightarrow R_Y$, (v) $R_V \wedge R_7 \rightarrow R_Z$. In brief, the wooden toybox disassembly can start with either one of Screw 1, 2, 3 since there are not any objects stacked on top of them. Also, Screw 5, 6 and 7 are the last ones to be removed as they hold the weight of all the other components. In the remainder of this paper, the rectangular parts are taken away right after dismantling the adjacent screws so that the disassembly rules can be simplified as:

- Rule I: $R_1 \wedge R_2 \wedge R_3 \rightarrow R_4$
- Rule II: $R_4 \rightarrow R_5 \wedge R_6 \wedge R_7$

where Rule I indicates that Task 1, Task 2, and Task 3 must be processed before Task 4; Rule II shows that Task 4 must be completed before working on Task 5, Task 6, and Task 7.

2) Cost of operations with human operator and robot: For obtaining the optimal disassembly sequence, each disassembly action needs to be parameterized. It is reasonable to quantify the disassembly cost as the combination of the travel distances between the robot/human operator and the to-be-disassembled components, as well as time spent on the tasks.

3) Safety of human operator: There is an assumption that removing hazardous materials would appear in the disassembly process. To prevent human injuries, the task planner in this instance should assign the robot to disassemble the component instead of the human operator. Therefore, safety constraints should be addressed regardless of the disassembly cost. We also assign disassembly tasks to the human operator and the robot sequentially [53] to avoid accidental collisions between the robot and the human operator. By explicitly considering the human operator's safety regarding hazardous materials in sequence planning, we expect that existing related hazard analysis and risk assessment requirements can be released such that HRC can be applied to broader industrial applications.

4) Computational cost: We refer to a previous study [44] in which an optimal disassembly sequence is conducted to minimize the total disassembly cost from the initial point to the last point. This strategy is only feasible in the situation of a small quantity of components to be disassembled. As the number of disassembly tasks grows, so does the time to search for the optimal sequence.

5) Human behavior: The disassembly efficiency would be significantly degraded if the human operator is frequently interfered in the planned trajectories. Hence, robots should be able to understand human's movement and such "understanding" should be considered in the sequence planning.

III. Real-time HBP

In this section, we focus on how to quantify human motion intention and how to leverage deep learning techniques for HBP.

A. Human movement intention

Many studies show that (1) the human operator would keep a comfortable distance from the robot [54], [55] and (2) the human operator tends to move toward the unfinished tasks after completing a task. In this paper, we adopt the behaviors for human intention prediction. These human behaviors result in varying traveling time after performing a task and would affect the human operator's real-time operation cost, thus they should be considered accordingly in solving the optimization problem.

We illustrate such movement intentions using two cases shown in Fig. 3 and Fig. 4, where the black circles, the gray-scaled circles, and the gray-scaled human icons denote the tasks to be performed, finished tasks and the previous positions of the human operator, respectively.

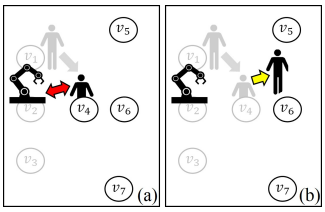

Fig. 3: Human behavior in disassembly sequence: Case I

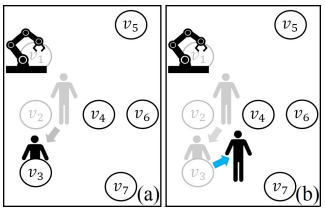

Fig. 4: Human behavior in disassembly sequence: Case II

In Case I, the initial positions of the human operator and the robot are near tasks v_1 and v_2 respectively and then the human operator is assigned to task v_4 (see Fig. 3a). After v_4 is performed, considering that the human operator is uncomfortable about the close proximity to the robot, the human operator would move in the direction away from the robot (see Fig. 3b). Such human behavior is quantified as below:

$$\angle \text{ Predicted direction after disassembling task } i$$
$$\sim(\text{Angle between robot and positive real axis}) \pm \pi$$

where $\sim$ means "related to", and the addition of π indicates that the human operator would move in the opposite direction from the robot. In Case II, the initial positions of the human operator and the robot locate near tasks v_2 and v_1 respectively and the human operator is assigned to task v_3 (see Fig. 4a). After task v_3 is finished, the human operator tends to prepare for the remaining tasks v_4, v_5, v_6 and v_7 (see Fig. 4b) and move toward the average direction of the four tasks. The average direction is estimated below:

$$\angle \text{ Predicted direction after disassembling task } i$$
$$\sim\frac{\sum(\text{Angles between unfinished tasks and task } i)}{\text{number of unfinished tasks}}$$

Noting that i is denoted as the task number, which is "3" in this example. Furthermore, the detailed illustration of calculating the average direction from task v_3 is shown in Fig. 5(a), where the blue human icon indicates the estimated position of the human operator. The predicted human position $q_3^{h'}$ after performing task v_3 is calculated as: $\angle q_3^{h'} = (\theta_{v_4}^{v_3} + \theta_{v_5}^{v_3} + \theta_{v_6}^{v_3} + \theta_{v_7}^{v_3})/4$, where $\theta_{v_4}^{v_3}$, $\theta_{v_5}^{v_3}$, $\theta_{v_6}^{v_3}$ and $\theta_{v_6}^{v_3}$ are denoted as the angles between task v_3 and tasks v_4, v_5, v_6, v_7, respectively.

B. Deep learning based human behavior predictor

It is challenging to predict human motion purely based on the above movement pattern since there are considerable uncertainties, and the disassembly scenarios are numerous according to the combination of the positions of the tasks, the human operator, and the robot. It is needed to find a way to predict human motion reasonably and efficiently. In recent years, the convolutional neural network (CNN) technique has been widely applied in image-based industrial tasks [56]–[58] since it can efficiently extract the significant features of the image without any human supervision [59]. More importantly, compared to other deep learning techniques, i.e., recurrent neural network, the convolution operation of the CNN filter enables the spatial information of the disassembly scene to be effectively captured [60]. The captured spatial information, i.e., the relative positions of the workers and the to-be-disassembled components also assist the network to make a more reasonable decision for the hand moving directions. Hence, we leverage the CNN technique and train a deep learning network model for HBP.

To train such a neural network, we divide the human operator's directions into eight after finishing the task v_x where $x \in \mathbb{Z}^+$, as illustrated in Fig. 5(b). It is noted that the number of human operator's directions can be infinite but it is reduced to eight to simplify and speed up the deep learning training process in this paper. We create the task planning scenarios for training the neural network model. The scenarios are saved as images, as illustrated in Fig. 6, containing the information of positions of the finished tasks (gray dots), the unfinished tasks (black dots), the robot (red dot) and the task to be assigned to the human operator (blue dot). We use these scenario images to represent various cases and stages of the disassembly.

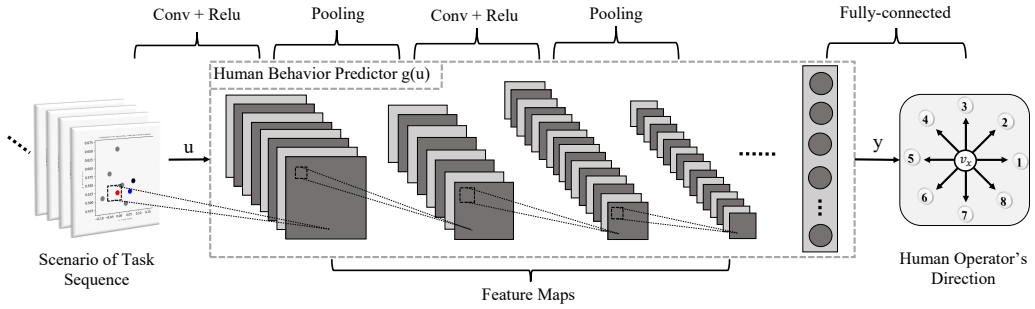

Fig. 7: The structure of CNN

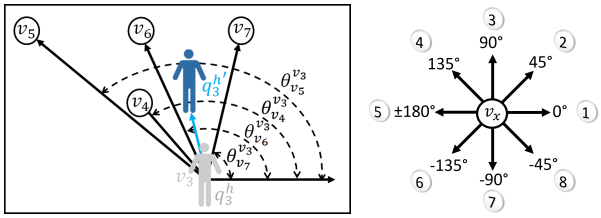

(a) An example of movement direction (blue arrow) of the human operator after disassembling task v_3

(b) Possible directions of the human operator

Fig. 5: Human motion direction

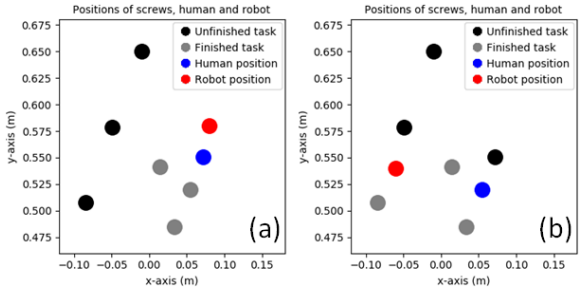

Fig. 6: Two examples of the scenario images

These scenario images are the inputs (denoted as u) of the CNN-based human behavior predictor. Fig. 7 illustrates the structure of the CNN. Each image is composed of three digital channels that are represented by matrices. A learning kernel convolves over the scenario images with a certain stride value to capture the important feature of the scenario images by getting dot product in the convolutional layer with the equation:

$$M(x,y) = \sum_{u=0}^{a-1}\sum_{v=0}^{b-1} k(u,v)I(x+u, y+v)$$

where M is the extracted feature map, k is an $a \times b$ kernel, and I is the scenario image. The Relu layer employs an activation function to set all negative values to be zero, which guarantees that not all neurons can be activated and further improves the computational efficiency. To reduce the computational cost in the training process, the pooling layer is implemented to decrease the dimension of feature maps. Pooling separates the feature map into spatially continuous matrices with the same dimension. Each matrix is replaced by its maximum element or the average value of elements.

To utilize the extracted feature more straightforwardly, the fully-connected part uses the Softmax function to transfer the feature map in Eq. (III-B) to 8×1 score vector which is corresponding to the 8 hand moving directions. The ground truth hand moving direction and the network prediction are labeled as D and $\hat{D}$, respectively. The training loss is defined as below:

$$Loss = -\frac{1}{Q}\sum_{n=1}^{Q}\sum_{i=1}^{k} B_{n,i}\{D \neq \hat{D}\}\log\left(P_{n,i}\right)$$

where Q is the observation number of training sample, k is the number of hand moving directions, $B_{n,i}$ is the binary indicator for the hand moving direction i regarding the training scenario image n, and $P_{n,i}$ indicates the probability score. After the whole training process, the well-trained network as human behavior predictor $g(u)$ has the capability to provide an anticipatory moving direction y with the highest possible score according to an image of a task sequence scenario.

To generalize human movement scenarios, the manipulators position is randomly given in the training set, a number of possible scenarios of the disassembly are generated as training images. A total of 10584 scenario images have been labeled with eight possible moving directions. Approximately 70% of images are in the training dataset (around 7408 images), and 15% are in the validation dataset (about 1588 images). The remaining 15% images constitute the test dataset. After the training process, the test data accuracy is 78.4%.

IV. Sequence Planner

This section introduces details of the sequence planner. The planner incorporates real-time human motion detection and prediction as well as safety constraints and disassembly rules. The planning problem is formulated into an optimization problem and solved in a receding-horizon way. The parameters and notations are listed in Table I, including parameters related to disassembly scenarios, disassembly cost, disassembly rules and decision variables. Two sets of decision variables are presented in Eq. (1): α_{ij} determines if task v_j is assigned to the human operator or the robot, and ϕ_{ij} determines if task v_i is conducted before task v_j. Next, the sequence planner is formulated into the following optimization problem, of which the cost function is defined as the disassembly cost.

Optimization problem:

$$\min_{\alpha_{ij},\phi_{ij}} \sum_{j=0}^{T}\sum_{i=0}^{T} \begin{bmatrix} h_{ij} & r_{ij} \end{bmatrix} \begin{bmatrix} 1-\alpha_{ij} \\ \alpha_{ij} \end{bmatrix} \phi_{ij} \tag{1}$$

Constraints:

$$\alpha_{ij} \in \{0,1\} \tag{2}$$

$$\phi_{ij} \in \{0,1\} \tag{3}$$

$$\sum_{i=0}^{T}\left[\sum_{j=0}^{T}\phi_{ij} - \sum_{k=0}^{T}\phi_{ki}\right] = 0 \tag{4}$$

$$\sum_{i=0}^{T}\sum_{j=0}^{T}\phi_{ij} = T \tag{5}$$

$$\alpha_{ij} = 1 \quad \text{when task } v_j \text{ is not safe for human operator} \tag{6}$$

$$\sum_{j\in V_i^b}\phi_{ji} + \sum_{k\in V_i^a}\phi_{ik} = 0 \tag{7}$$

$$h_{ij} = \left|q_i^h - P(v_j)\right| + \tau S^h(v_j) \tag{8}$$

$$r_{ij} = \left|q_i^r - P(v_j)\right| + \tau S^r(v_j) \tag{9}$$

The constraints are explained in detail as follows. Constraint (2) guarantees that each task can be done by one human operator or one robot. Constraints (3) and (4) prevent each disassembly task from being performed more than once. In particular, the two summation terms inside the bracket of Constraint (4) ensure (i) the same number of workflow entering/exiting the same task excluding the starting task and the ending task, and (ii) the same number of workflow exiting/entering the starting/ending task. Constraint (5) makes sure that all tasks (v_1, v_2, ..., v_T) are executed.

Next, we conduct Constraint (6) to ensure human safety in the disassembly process: if task v_j is labeled as unsafe for human operation, the decision variable α_{ij} is set to 1, forcing the robot to perform task v_j. In addition, Constraint (7) guarantees the obedience of the precedence relations among disassembly parts, following the disassembly rules. Take the toybox disassembly from Fig. 1b as an example, if tasks v_1, v_2, v_3 must be performed before task 4 followed by tasks v_5, v_6, v_7, then $j \in \{1,2,3\}$ and $k \in \{5,6,7\}$, such that $\sum_{j\in\{1,2,3\}}\phi_{j4} + \sum_{k\in\{5,6,7\}}\phi_{4k} = 0$.

Also, we explicitly consider the HRC setting by defining the cost function in Eq. (1), where h_{ij} and r_{ij} denote the cost of operation with the human operator and the robot respectively, which are presumably defined in Constraints (8) and (9). There are two terms in each of the aforementioned constraints: the first term represents the distance between task v_j and the worker after leaving task v_i, and the second term indicates the worker's effort spent on task v_j. The two terms are summed using the weighting factor τ.

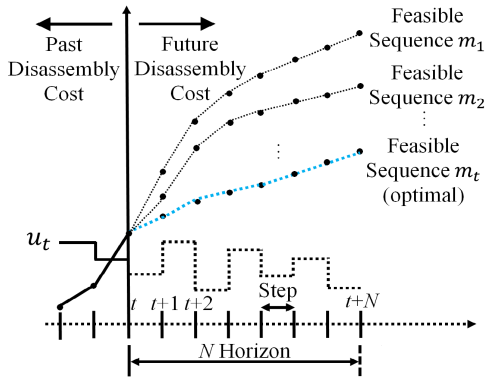

Fig. 8: Receding horizon of sequence planning

Despite the non-dynamic feature in sequence planning, we introduce the concept of state-feedback control law (referring to Fig. 8) into the optimization problem and solve it in a receding-horizon way; (i) the "performance index" in Eq. (10), which is minimized at each step, explicitly considers the distances between disassembly tasks and the positions of the human operator or the robot; (ii) the "constraints" of the RHC correspond to safety conditions for human operation and disassembly rules; (iii) the "states" of the disassembly sequence contain the set of remaining disassembly tasks $V(t)$ and the positions of the human operator q_t^h and the robot q_t^r. The parameters related to the receding horizon and states of the task sequence are shown in Table II.

(a) Disassembly Scenarios

Symbol	Definition
T	The number of total disassembly tasks, $T \in \mathbb{Z}^+$.
v_i	The index of disassembly tasks.
$P(v_j)$	Position of the task v_j.

(b) Disassembly Cost

h_{ij}	Human operator's disassembly cost from v_i to v_j.
r_{ij}	Robot's disassembly cost from v_i to v_j.
q_i^h	Position of the human operator after completing v_i.
q_i^r	Position of the robot after completing v_i.
$S^h(v_j)$	Human operator's labor effort spent on task v_j.
$S^r(v_j)$	Robot's labor effort spent on task v_j.
τ	Weighting factor in the disassembly cost quantification.

(c) Disassembly Rules

V_i^b	Task set that must be done before v_i.
V_i^a	Task set that needs to be done after v_i.

(d) Decision Variables

ϕ_{ij}	"1" if v_j is conducted immediately after v_i; "0" Otherwise.
α_{ij}	"1" if v_j is assigned to the robot; "0" if v_j is assigned to the human operator.

TABLE I: Parameters related to the disassembly: (a) scenarios, (b) cost, (c) rules and (d) decision variables

(a) Receding Horizon

Symbol	Definition
t	Current step of performing a disassembly task, $t \le T$.
N	Length of the preview horizon.

(b) States

$V(k)$	Remaining task(s) at step k.
$v(k)$	Task completed at step k.
$\hat{q}_p^h(k)$	Predicted human position after task p at step k

TABLE II: Parameters related to (a) receding horizon, (b) states

Receding-Horizon Strategies:

$$\min_{\phi_{pm},\alpha_{pm}} \sum_{k=t}^{t+N-1} \begin{bmatrix} h_{pm}(k) & r_{pm}(k) \end{bmatrix} \begin{bmatrix} 1-\alpha_{pm} \\ \alpha_{pm} \end{bmatrix} \phi_{pm} \tag{10}$$

s.t.

$$\phi_{pm}, \alpha_{pm} \in \{0,1\} \tag{11}$$

$$p \in v(k) \quad k = t, ..., t+N-1 \tag{12}$$

$$m \in V(k) \tag{13}$$

$$h_{pm}(k) = \left|\hat{q}_p^h(k) - P(v_m)\right| + \tau S^h(v_m) \tag{14}$$

$$r_{pm}(k) = \left|q_p^r(k) - P(v_m)\right| + \tau S^h(v_m) \tag{15}$$

$$\hat{q}_p^h(k) \text{ is predicted by the deep learning model} \tag{16}$$

$$V(k+1) = F_v\{V(k), v(k), \phi_{pm}(k), \alpha_{pm}(k)\} \tag{17}$$

$$\hat{q}_p^h(k+1) = F_h(q_p^h(k), \phi_{pm}(k), \alpha_{pm}(k)) \tag{18}$$

$$\hat{q}_p^r(k+1) = F_r(q_p^r(k), \phi_{pm}(k), \alpha_{pm}(k)) \tag{19}$$

We exploit the resemblance between RHC and the proposed local optimal sequence planner in this paper. After executing a disassembly task at each step, the set $V(t)$ is updated and the human operator may move to a different position, yielding a new

position q_t^h. The optimal disassembly sequence over N steps is derived but only the first control action is applied: $\{\phi_{pm}, \alpha_{pm}\}$, where $p = v(k)$ is the task done at step k and $m \in V(k)$ where $V(k)$ is the index of the remaining task set, as shown in Constraints (11) to (13). Meanwhile, Constraints (14) and (15) are similar to Constraints (8) and (9) except for the estimated states $\hat{q}_p^h(k)$ and $\hat{q}_p^r(k)$, which indicate the predicted positions of the human operator and the robot respectively after performing task m at step k. At step $k+1$, the new remaining task set $V(k+1)$ is updated as shown in Constraint (17) and the optimization is repeated. Also, F_v, F_h and F_r in Constraints (17) to (19) denote the "Functions" of the corresponding states and decision variables to predict the remaining tasks and the positions of the human operator and the robot, respectively. By using RHC, the real-time human motion can be explicitly included and the optimization problem can be solved at each step without excessive computational cost. Fig. 9 depicts the overview of the proposed receding-horizon disassembly planner.

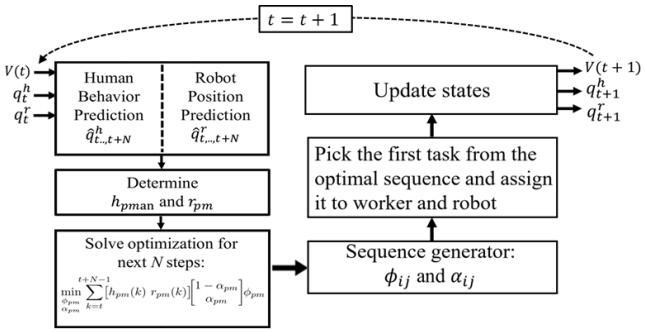

Fig. 9: Sequence generation and optimization of the proposed N-step disassembly sequence planner

V. Experimental Validation

This section presents the validation of the proposed HRC disassembly sequence planner. The test equipment is shown in Fig. 10, consisting of (i) requisite cameras used to identify the positions of to-be-disassembled objects, the robot and the human operator, (ii) a universal robot (UR) collaborating with the human operator, and (iii) a Linux Operating System with an Intel Core i7 CPU and an Nvidia GTX 1050 Ti GPU. It is expected that the human operator would stay alongside the robot to inspect and accomplish the disassembly tasks collaboratively. In addition, all the to-be-disassembled objects are assumed to be reachable by the robot and the human operator with two variables given: the orientation and components unsafe for human operation.

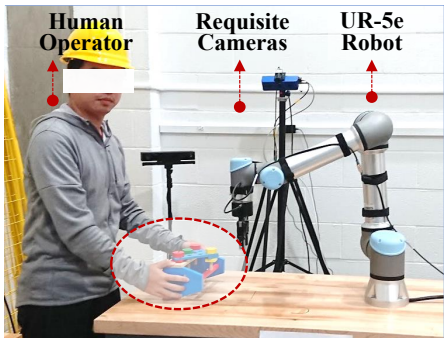

Fig. 10: Experimental test setup

Case Study I: Toybox with Screw 7 as the Unsafe Condition

At the beginning of the experiment, the toybox is randomly placed on the table and the positions of the robot, the human operator and the to-be-disassembled components are identified by the camera and sent to the computer for sequence planning. Faster recurrent-CNN (Faster R-CNN) [61], a mature multi-target detection algorithm based on deep learning [62] is used to generate a series of bounding boxes to classify and locate the objects simultaneously. The deep learning model is trained with 220 images of 660 manually labeled objects.

Next, the positions of the screws ($P(v_{i,..,7})$), the robot (q_t^r), the human operator (q_t^h), and the remaining screws to be disassembled (V_t) are used as the initial states of RHC at each step t ($t = 1, 2, ..., 7$, see Fig. 1b and Table II(a)). The task planner searches for the next N-step feasible sequences, and the control action is obtained by solving the optimal sequence problem at each step instantly online. Then, the first task of the optimal control sequence is executed by the human operator or the robot as assigned. The procedure repeats for the next steps until all the screws are disassembled. Noting that Screw 7 is painted in red to emulate the unsafe condition in this study.

In the first disassembly round, the position data of the wooden screws, the human operator and the robot is processed to find the optimal disassembly sequence, as illustrated in Fig. 11a(ii). Afterward, the planner generates the next three-step optimal control sequence as shown in Fig. 11a(iii), where (1) the blue arrow indicates the first disassembly task and the corresponding worker (the robot), (2) the long gray arrow denotes the second optimal sequence and the corresponding worker, the human operator in this step, (3) the blue hand icon depicts the predicted position of the human hand after disassembling Screw 2, (4) the two short gray arrows indicate the movements of the human hand after Screw 2 and toward Screw 1 respectively. The round is complete by the robot removing Screw 3, as shown in Fig. 11a(iv).

In the second round, the optimization process repeats by firstly acquiring the position information (see Fig. 11b(i) and Fig. 11b(ii)), followed by generating the optimal sequence in Fig. 11b(iii) and then predicting the human hand's position for the next round. Also, the first part of the optimal control sequence is applied such that the disassembly of Screw 1 is assigned and executed by the human operator as in Fig. 11b(iii) and Fig. 11b(iv). Next, the third disassembly task and the corresponding worker are determined (see Fig. 11c) by the following three-step optimal disassembly sequence: the human operator removing Screw 2, followed by the robot dismantling Screw 4, and then the human operator disassembling Screw 6. It is worth noting that the sequence planner only sends out the first task with the corresponding worker from the optimal sequence for execution. In round 4, the following optimal sequence is found: the robot removes Screw 4 (the blue one) and then Screw 5, followed by the human operator removing Screw 6, as shown in Fig. 11d. Consequently, Screw 4 and the robot in the first optimal sequence are determined as the disassembly task and the corresponding worker.

In round 5, the optimal sequence is obtained with the human operator disassembling Screw 6, followed by the robot dismantling Screw 7 and Screw 5 sequentially, as illustrated in Fig. 11e.

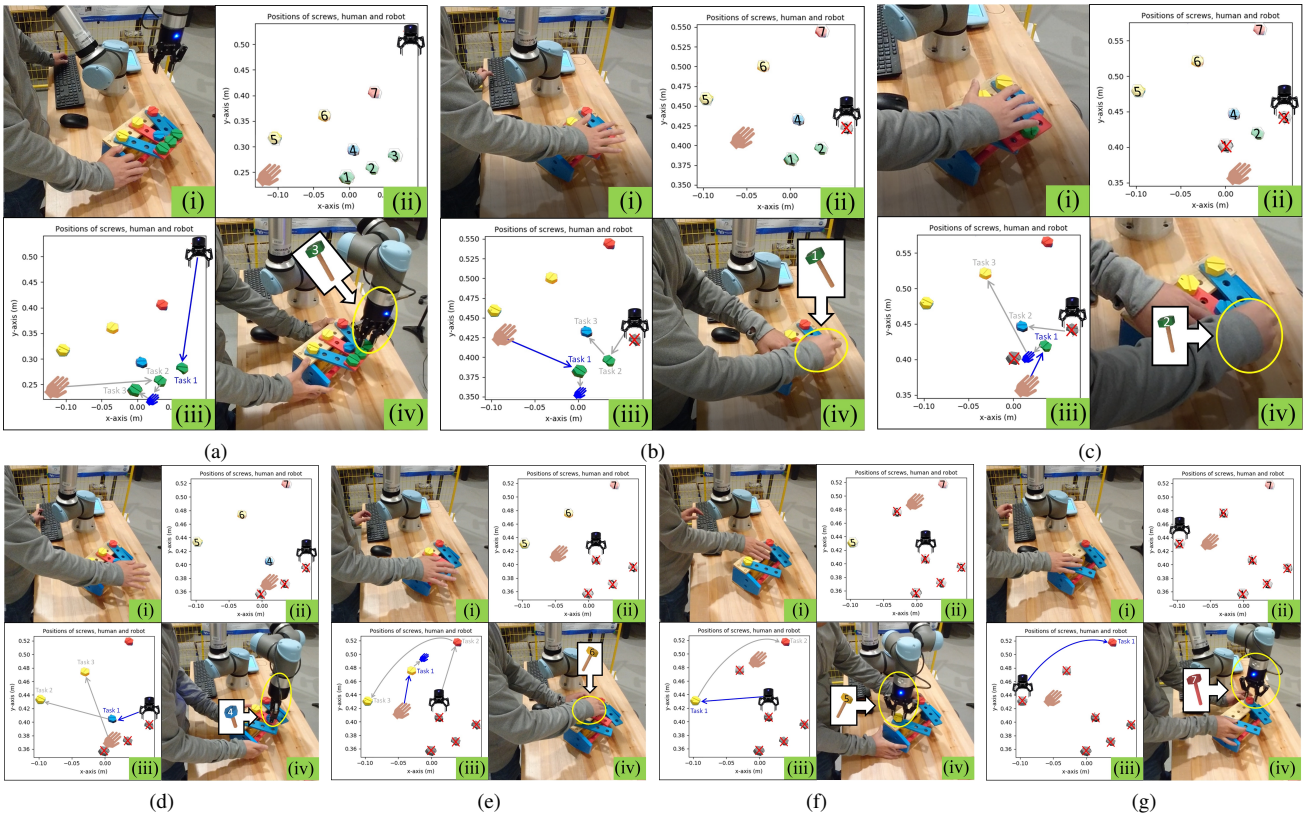

Fig. 11: Case I (a) round 1: robot is assigned to Screw 3, (b) round 2: human is assigned to Screw 1, (c) round 3: human is assigned to Screw 2, (d) round 4: robot is assigned to Screw 4, (e) round 5: human is assigned to Screw 6, (f) round 6: robot is assigned to Screw 5, (g) round 7: robot is assigned to Screw 7

Screw 6 is then chosen and disassembled by the robot. Noting that there are only two remaining tasks in the following disassembly rounds. The optimal sequence at round 6 is Screw 5 and Screw 7 being executed by the robot in sequence (see Fig. 11f). The round is complete after assigning the disassembly of Screw 5 to the robot.

In the final task, because Screw 7 is labeled as unsafe for human operation, it is assigned to the robot disregarding that the robot's disassembly cost is higher than that of the human operator. In other words "1" is forcibly assigned to the decision variable α_{i7} used in Fig. 11g, where $i = 1, 2, ...6$.

Case Study II: HDD with Task 2 as the Unsafe Condition

A simplified HDD disassembly is used to validate the proposed HRC disassembly sequence planner. The experiment setup is similar to Case Study I (see Fig. 10) with a used HDD (see Fig. 12a) and a hand tracking feature from Google Mediapipe [63], a powerful finger tracking solution that tracks 21 joints on a human hand from just one video frame. Also, the precedence relationships of the 15 sub-assemblies are shown in Fig. 12b, in which tasks with bidirectional arrows indicate no precedence relationships among the linked tasks. It is assumed that the workers tend to finish one disassembly module (see Table III) before moving to the next. The whole disassembly comes to the end when Components 1 to 14 are all removed from the HDD base (see Component 15 in Fig. 12b). In this case study, the hand tracking function is used to measure the distances between the to-be-disassembled components. Additionally, it is assumed that the positions of all the 14 components (see Fig. 12b) are given, and Task 2 is marked as unsafe for human operation and highlighted in red, as shown in Fig. 13a(ii).

Module	Task No.	Disassembly Task
Actuator	Task-1	Top Actuator
	Task-2	Actuator Arm
	Task-3	Bottom Actuator Screw-1
	Task-4	Bottom Actuator Screw-2
	Task-5	Bottom Actuator Screw-3
	Task-6	Bottom Actuator
Platter	Task-7	Spindle Screw-1
	Task-8	Spindle Screw-2
	Task-9	Spindle Screw-3
	Task-10	Spindle
	Task-11	Platter
Chip	Task-12	Chip Screw-1
	Task-13	Chip Screw-2
	Task-14	Chip

TABLE III: Disassembly modules, disassembly task numbering and names of the used HDD (see Fig. 12)

Initially, the used HDD is placed on the desk as shown in Fig. 13a(i). Then, the positions of the human operator, the robot and the 14 to-be-disassembled components are collected for sequence planning, as depicted in Fig. 13a(ii). Afterward, the planner generates the optimal control sequence for the next three steps as shown in Fig. 13a(iii), where (1) the blue arrow indicates the first disassembly task and the corresponding worker (the human operator) obtained from the optimal control sequence, (2) the long gray arrow denotes the second optimal sequence and the corresponding worker, the robot in this step; (3) the blue hand icon depicts the predicted position of the human hand after performing Task 1; (4) the two short gray arrows indicate the

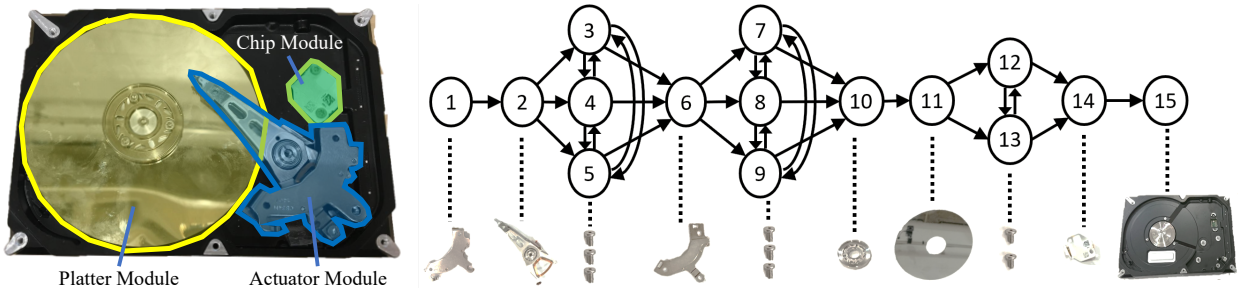

(a) (b)

Fig. 12: (a) A used HDD and (b) the components' precedence relationships with their disassembly task numbers

human operator's movement after Task 1 and the robot's next task (Task 4) after performing Task 2, sequentially. Then, the sequence planner completes the first round by assigning the human operator to Task 1 as demonstrated in Fig. 13a(iv). The finished task is labeled with a red cross sign as shown in Fig. 13b(ii).

In round 2, the sequence planner firstly updates the 13 remaining tasks and the positions of the robot and the human operator shown in Fig. 13b(i) and Fig. 13b(ii), and then it generates the optimal sequence in Fig. 13b(iii) and predicts the human hand's position for the next round. The first part of the optimal control sequence is applied so that the robot is assigned to perform Task 2, the unsafe task. Even though the human's position is closer to Task 2, the robot is sent to finish the task because of the unsafe condition. In other words, the decision variables α_{i2} in this situation are set to "1" (see Eq. (10)), forcing the robot to execute Task 2. Next, similar to previous rounds, the sequence planner firstly locates the workers' positions and the 12 remaining tasks. Fig. 13c shows the process of determining the task and the worker for round 3. The following optimal sequence is found: Task 4, followed with Task 5, and then Task 3 all by the human operator. The robot remains at the same position as in round 2. Lastly, the sequence planner extracts the first of these three tasks from the optimal sequence and then executes it with the human operator. For the optimal sequence at round 4, Task 3 is performed by the human operator, followed by Task 5 and then Task 6, as shown in Fig. 13d(iii). The human operator is determined to perform the current and the future tasks because of both the shorter distances between Task 3, Task 5 and Task 6, and the lower labor efforts in these three tasks.

At round 5, we intend to move the human operator away from the predicted position from round 4 to observe the change of the predicted disassembly sequence. The following optimal sequence is obtained: the robot being assigned to Task 5, followed by the human operator being assigned to Task 6 and Task 9 sequentially, as shown in Fig. 13e. Compared to the prediction from round 4, the robot is assigned to Task 5 instead of the human operator, as the actual human movement is different from the prediction. The fifth disassembly round ends by assigning the robot to Task 5, as picked from the first sequence of the optimal sequence. In round 6, the human operator moves slightly to the right near Task 8. The following optimal sequence is obtained and depicted in Fig. 13f: the human operator executes Task 6, Task 8 and Task 7 in sequence. This round is complete after assigning Task 6 to the human operator.

There are two remaining disassembly modules (Task 7 to Task 11 for platter module and Task 12 to Task 14 for chip module, see Table III) left at disassembly round 7. The human operator in this round does not move to the lastly predicted direction, generating the optimal sequence as follows: Task 9 followed with Task 8 and then Task 7 all to be performed by the human operator, as shown in Fig. 13g. After round 7, the human operator stays closer to direction 3 instead of direction 6 (see Fig. 5(b) and Fig. 13h(ii)) from the previous prediction. Despite the prediction error, the task planner updates the new position of the human operator and generates the new optimal sequence for round 8: the robot for Task 8, followed by the human operator for Task 7 and Task 10 as illustrated in Fig. 13h.

The optimal sequence at round 9 is Task 7 to be performed by the human operator, followed by Task 10 to be executed by the robot, and then Task 11 disassembled by the human operator (see Fig. 13i). Even though both the human operator and the robot are close to Task 7 with similar distance measures, since the disassembly cost with the human operator is lower than that with the robot, the task is assigned to the human operator. It is worth mentioning that instead of moving to the predicted direction 5 (see Fig. 13i(ii)), after performing Task 7, the human operator moves to direction 4 (see Fig. 13j(ii)), which is one-direction different (see Fig. 5(b)) from the prediction. Despite the prediction error, the human operator's position is still close to the expected position. In round 10, the robot executes Task 10 as in Fig. 13j(iii), which is accurately predicted in round 9 (see Fig. 13i(iii)). Then the human operator moves slightly to the right after Task 10. Since the distances between the remaining tasks have not changed significantly, the human operator is assigned to Task 11 in round 11, as predicted in round 10.

At round 12, the human moves closer to the remaining tasks. Although the robot has a lower labor effort than the human operator on Task 13 (see Fig. 13l), the human operator is assigned to the task because of the shorter travel distance that contributes to the lower disassembly cost. In round 13, because Task 12 must precede before Task 14 and the disassembly cost is lower with the robot than the human operator, Task 12 is assigned to the robot. The optimal sequence at disassembly round 13 is depicted in Fig. 13m(iii). Noting that the disassembly cost includes not only the distance between the worker and the to-be-disassembled object but also the labor effort of the disassembly Task. The last task is to perform Task 14. Because the human operator (see Fig. 13n(i) and Fig. 13n(ii)) remains at the same position as at round 13, the disassembly cost does not change. Since the human operator's disassembly cost is lower, the human operator is assigned to the last task.

In summary, two case studies have been conducted for the validation. The first case study shows that the proposed sequence planner effectively predicts the human operator's standby po-

Fig. 13: Case II (a) Round 1: human operator for Task 1, (b) Round 2: robot for unsafe Task 2, (c) Round 3: human operator for Task 4, (d) Round 4: human operator for Task 3, (e) Round 5: robot for Task 5, (f) Round 6: human operator for Task 6, (g) Round 7: human operator for Task 9, (h) Round 8: robot for Task 8, (i) Round 9: human operator for Task 7, (j) Round 10: robot for Task 10, (k) Round 11: human operator for Task 11, (l) Round 12: human operator for Task 13, (m) Round 13: robot for Task 12, (n) Round 14: human operator for Task 14

sitions after finishing a disassembly task, which has been used as a factor in the disassembly cost in Constraint (14). Also, the planner assigns the unsafe tasks to the robot while minimizing the disassembly completion time. The second case study demonstrates the disassembly of the simplified HDD using the proposed HRC sequence planner, in which the human operator tends to move more randomly because of the narrow spaces between the smaller to-be-disassembled components. Despite the more unpredictable movements of the human operator, the proposed sequence planner reacts to the position change and generates new HRC task sequences to continue and finish the whole disassembly process successfully.

VI. Conclusions and future work

This paper presents a disassembly sequence planning in a human-robot collaboration setting with real-time human motion prediction. Multiple factors in the disassembly process have been considered, including real-time positions of the workers and the to-be-disassembled components, varying disassembly cost, human behavior prediction, and safety for human operation. The optimization problem is approached from a receding-horizon perspective considering real-time human motion. The disassembly of a wooden toybox and a used HDD are demonstrated to validate the proposed algorithm. The experiments show that the robot collaborates with the human operator and they efficiently complete the disassembly tasks together without breaking safety constraints and disassembly rules. It is to be noted that the disassembly objects used in this paper are prototype implementations with simple structures and small numbers of components. As part of future work, the algorithm will be made more efficient for the human operator with constraints related to ergonomics for instance. Also, extra experiments could be done with different operators to compare whether the algorithm makes the disassembly procedure convenient and user-friendly for wide industrial applications.

Acknowledgment

This material is based upon work supported by the National Science Foundation (NSF) - USA under Grants No. 2026533, No. 2026276 and No. 1928595. Any opinions, findings, and conclusions or recommendations expressed in this material are those of the authors and do not necessarily reflect the views of the NSF.

References

[1] A. F. Lambert and S. M. Gupta, *Disassembly modeling for assembly, maintenance, reuse and recycling*. CRC press, 2004.

[2] A. Cesta, A. Orlandini, G. Bernardi, and A. Umbrico, "Towards a planning-based framework for symbiotic human-robot collaboration," in *2016 IEEE 21st International Conference on Emerging Technologies and Factory Automation (ETFA)*. IEEE, 2016, pp. 1–8.

[3] N. Shyamsundar and R. Gadh, "Selective disassembly of virtual prototypes," in *1996 IEEE International Conference on Systems, Man and Cybernetics. Information Intelligence and Systems (Cat. No. 96CH35929)*, vol. 4. IEEE, 1996, pp. 3159–3164.

[4] A. J. Lambert, "Disassembly sequencing: a survey," *International Journal of Production Research*, vol. 41, no. 16, pp. 3721–3759, 2003.

[5] X. Liu, G. Peng, X. Liu, and Y. Hou, "Disassembly sequence planning approach for product virtual maintenance based on improved max–min ant system," *The International Journal of Advanced Manufacturing Technology*, vol. 59, no. 5, pp. 829–839, 2012.

[6] K. Meng, P. Lou, X. Peng, and V. Prybutok, "An improved co-evolutionary algorithm for green manufacturing by integration of recovery option selection and disassembly planning for end-of-life products," *International Journal of Production Research*, vol. 54, no. 18, pp. 5567–5593, 2016.

[7] M. R. Bahubalendruni and V. P. Varupala, "Disassembly sequence planning for safe disposal of end-of-life waste electric and electronic equipment," *National Academy Science Letters*, vol. 44, no. 3, pp. 243–247, 2021.

[8] E. Kongar and S. M. Gupta, "Disassembly sequencing using genetic algorithm," *The International Journal of Advanced Manufacturing Technology*, vol. 30, no. 5-6, pp. 497–506, 2006.

[9] T. De Fazio and D. Whitney, "Simplified generation of all mechanical assembly sequences," *IEEE Journal on Robotics and Automation*, vol. 3, no. 6, pp. 640–658, 1987.

[10] C. Wang, M. Zheng, Z. Wang, C. Peng, and M. Tomizuka, "Robust iterative learning control for vibration suppression of industrial robot manipulators," *Journal of Dynamic Systems, Measurement, and Control*, vol. 140, no. 1, p. 011003, 2018.

[11] C. Wang, M. Zheng, Z. Wang, and M. Tomizuka, "Robust two-degree-of-freedom iterative learning control for flexibility compensation of industrial robot manipulators," in *2016 IEEE International Conference on Robotics and Automation (ICRA)*. IEEE, 2016, pp. 2381–2386.

[12] M. Hedelind and S. Kock, "Requirements on flexible robot systems for small parts assembly: A case study," in *2011 IEEE International Symposium on Assembly and Manufacturing*. IEEE, 2011, pp. 1–7.

[13] D. G. Luenberger, Y. Ye *et al.*, *Linear and nonlinear programming*. Springer, 1984, vol. 2.

[14] L. H. De Mello and A. C. Sanderson, "And/or graph representation of assembly plans," *IEEE Transactions on robotics and automation*, vol. 6, no. 2, pp. 188–199, 1990.

[15] E. R. Gansner, E. Koutsofios, S. C. North, and K.-P. Vo, "A technique for drawing directed graphs," *IEEE Transactions on Software Engineering*, vol. 19, no. 3, pp. 214–230, 1993.

[16] A. J. Lambert, "Determining optimum disassembly sequences in electronic equipment," *Computers & Industrial Engineering*, vol. 43, no. 3, pp. 553–575, 2002.

[17] M. Santochi, G. Dini, and F. Failli, "Computer aided disassembly planning: state of the art and perspectives," *CIRP Annals*, vol. 51, no. 2, pp. 507–529, 2002.

[18] S. M. McGovern and S. M. Gupta, "Ant colony optimization for disassembly sequencing with multiple objectives," *The International Journal of Advanced Manufacturing Technology*, vol. 30, no. 5-6, pp. 481–496, 2006.

[19] J. Krüger, T. K. Lien, and A. Verl, "Cooperation of human and machines in assembly lines," *CIRP annals*, vol. 58, no. 2, pp. 628–646, 2009.

[20] S. Makris, P. Karagiannis, S. Koukas, and A.-S. Matthaiakis, "Augmented reality system for operator support in human–robot collaborative assembly," *CIRP Annals*, vol. 65, no. 1, pp. 61–64, 2016.

[21] F. Ranz, T. Komenda, G. Reisinger, P. Hold, V. Hummel, and W. Sihn, "A morphology of human robot collaboration systems for industrial assembly," *Procedia CiRp*, vol. 72, pp. 99–104, 2018.

[22] G. Bruno and D. Antonelli, "Dynamic task classification and assignment for the management of human-robot collaborative teams in workcells," *The International Journal of Advanced Manufacturing Technology*, vol. 98, no. 9, pp. 2415–2427, 2018.

[23] F. Chen, K. Sekiyama, H. Sasaki, J. Huang, B. Sun, and T. Fukuda, "Assembly strategy modeling and selection for human and robot coordinated cell assembly," in *2011 IEEE/RSJ International Conference on Intelligent Robots and Systems*. IEEE, 2011, pp. 4670–4675.

[24] A. A. Malik and A. Bilberg, "Complexity-based task allocation in human-robot collaborative assembly," *Industrial Robot: the international journal of robotics research and application*, 2019.

[25] A. Bilberg and A. A. Malik, "Digital twin driven human–robot collaborative assembly," *CIRP Annals*, vol. 68, no. 1, pp. 499–502, 2019.

[26] Z. A. Çil, Z. Li, S. Mete, and E. Özceylan, "Mathematical model and bee algorithms for mixed-model assembly line balancing problem with physical human–robot collaboration," *Applied soft computing*, vol. 93, p. 106394, 2020.

[27] Q. Liu, Z. Liu, W. Xu, Q. Tang, Z. Zhou, and D. T. Pham, "Human-robot collaboration in disassembly for sustainable manufacturing," *International Journal of Production Research*, vol. 57, no. 12, pp. 4027–4044, 2019.

[28] H. Cheng, W. Xu, Q. Ai, Q. Liu, Z. Zhou, and D. T. Pham, "Manufacturing capability assessment for human-robot collaborative disassembly based on multi-data fusion," *Procedia Manufacturing*, vol. 10, pp. 26–36, 2017.

[29] B. Liu, W. Xu, J. Liu, B. Yao, Z. Zhou, and D. T. Pham, "Human-robot collaboration for disassembly line balancing problem in remanufacturing," in *ASME 2019 14th International Manufacturing Science and Engineering Conference*. American Society of Mechanical Engineers Digital Collection, 2019.

[30] I. Chatzikonstantinou, D. Giakoumis, and D. Tzovaras, "A new shopfloor orchestration approach for collaborative human-robot device disassembly," in *2019 IEEE SmartWorld, Ubiquitous Intelligence & Computing, Advanced & Trusted Computing, Scalable Computing & Communications, Cloud & Big Data Computing, Internet of People and Smart City Innovation*. IEEE, 2019, pp. 225–230.

[31] J. Huang, D. T. Pham, R. Li, M. Qu, Y. Wang, M. Kerin, S. Su, C. Ji, O. Mahomed, R. Khalil *et al.*, "An experimental human-robot collaborative disassembly cell," *Computers & Industrial Engineering*, vol. 155, p. 107189, 2021.

[32] M.-L. Lee, S. Behdad, X. Liang, and M. Zheng, "Task allocation and planning for product disassembly with human-robot collaboration," *Robotics and Computer-Integrated Manufacturing*, 2021.

[33] Y. Wang, X. Ye, Y. Yang, and W. Zhang, "Collision-free trajectory planning in human-robot interaction through hand movement prediction from vision," in *2017 IEEE-RAS 17th International Conference on Humanoid Robotics (Humanoids)*. IEEE, 2017, pp. 305–310.

[34] J. Mainprice and D. Berenson, "Human-robot collaborative manipulation planning using early prediction of human motion," in *2013 IEEE/RSJ International Conference on Intelligent Robots and Systems*. IEEE, 2013, pp. 299–306.

[35] J. F. Fisac, A. Bajcsy, S. L. Herbert, D. Fridovich-Keil, S. Wang, C. J. Tomlin, and A. D. Dragan, "Probabilistically safe robot planning with confidence-based human predictions," *arXiv:1806.00109*, 2018.

[36] J. Bütepage, H. Kjellström, and D. Kragic, "Anticipating many futures: Online human motion prediction and synthesis for human-robot collaboration," *arXiv:1702.08212*, 2017.

[37] J. Zhang, H. Liu, Q. Chang, L. Wang, and R. X. Gao, "Recurrent neural network for motion trajectory prediction in human-robot collaborative assembly," *CIRP Annals*, 2020.

[38] V. V. Unhelkar, P. A. Lasota, Q. Tyroller, R.-D. Buhai, L. Marceau, B. Deml, and J. A. Shah, "Human-aware robotic assistant for collaborative assembly: Integrating human motion prediction with planning in time," *IEEE Robotics and Automation Letters*, vol. 3, no. 3, pp. 2394–2401, 2018.

[39] C. Pérez-D'Arpino and J. A. Shah, "Fast target prediction of human reaching motion for cooperative human-robot manipulation tasks using time series classification," in *2015 IEEE international conference on robotics and automation (ICRA)*. IEEE, 2015, pp. 6175–6182.

[40] J. Mainprice, R. Hayne, and D. Berenson, "Goal set inverse optimal control and iterative replanning for predicting human reaching motions in shared workspaces," *IEEE Transactions on Robotics*, vol. 32, no. 4, pp. 897–908, 2016.

[41] C.-M. Huang and B. Mutlu, "Anticipatory robot control for efficient human-robot collaboration," in *2016 11th ACM/IEEE international conference on human-robot interaction*. IEEE, 2016, pp. 83–90.

[42] H. Liu and L. Wang, "Human motion prediction for human-robot collaboration," *Journal of Manufacturing Systems*, vol. 44, pp. 287–294, 2017.

[43] K. P. Hawkins, N. Vo, S. Bansal, and A. F. Bobick, "Probabilistic human action prediction and wait-sensitive planning for responsive human-robot collaboration," in *2013 13th IEEE-RAS International Conference on Humanoid Robots (Humanoids)*. IEEE, 2013, pp. 499–506.

[44] M.-L. Lee, X. Liang, S. Behdad, and M. Zheng, "Disassembly sequence planning considering human-robot collaboration," in *2020 American Control Conference*, Denver, CO, USA, July 2019.

[45] F. Torres, S. Puente, and C. Díaz, "Automatic cooperative disassembly robotic system: Task planner to distribute tasks among robots," *Control Engineering Practice*, vol. 17, no. 1, pp. 112–121, 2009.

[46] S. P. Mendez, F. T. Medina, and J. P. Baeza, "Product disassembly scheduling using graph models," in *Environmentally Conscious Manufacturing II*, vol. 4569. International Society for Optics and Photonics, 2002, pp. 63–70.

[47] F. Allgöwer and A. Zheng, *Nonlinear model predictive control*. Birkhäuser, 2012, vol. 26.

[48] M.-L. Lee, S. Behdad, X. Liang, and M. Zheng, "A real-time receding horizon sequence planner for disassembly in a human-robot collaboration setting," *arXiv:2007.02981*, 2020.

[49] W. Wang, R. Li, Y. Chen, and Y. Jia, "Human intention prediction in human-robot collaborative tasks," in *2018 ACM/IEEE international conference on human-robot interaction*, 2018, pp. 279–280.

[50] B. Reily, F. Han, L. E. Parker, and H. Zhang, "Skeleton-based bio-inspired human activity prediction for real-time human–robot interaction," *Autonomous Robots*, vol. 42, no. 6, pp. 1281–1298, 2018.

[51] A. D. Dragan and S. S. Srinivasa, *Formalizing assistive teleoperation*. MIT Press, July, 2012.

[52] A. Güngör and S. M. Gupta, "Disassembly line in product recovery," *International Journal of Production Research*, vol. 40, no. 11, pp. 2569–2589, 2002.

[53] K. Brown, O. Peltzer, M. A. Sehr, M. Schwager, and M. J. Kochenderfer, "Optimal sequential task assignment and path finding for multi-agent robotic assembly planning," in *2020 IEEE International Conference on Robotics and Automation (ICRA)*. IEEE, 2020, pp. 441–447.

[54] Y. Niu, F. Schulte, and R. R. Negenborn, "Human aspects in collaborative order picking–letting robotic agents learn about human discomfort," *Procedia Computer Science*, vol. 180, pp. 877–886, 2021.

[55] W. Wang, Y. Chen, R. Li, and Y. Jia, "Learning and comfort in human–robot interaction: A review," *Applied Sciences*, vol. 9, no. 23, p. 5152, 2019.

[56] Q. Gao, J. Liu, Z. Ju, Y. Li, T. Zhang, and L. Zhang, "Static hand gesture recognition with parallel cnns for space human-robot interaction," in *International Conference on Intelligent Robotics and Applications*. Springer, 2017, pp. 462–473.

[57] X. Li, M. Li, Y. Wu, D. Zhou, T. Liu, F. Hao, J. Yue, and Q. Ma, "Accurate screw detection method based on faster r-cnn and rotation edge similarity for automatic screw disassembly," *International Journal of Computer Integrated Manufacturing*, pp. 1–19, 2021.

[58] W. Liu, Z. Chen, and M. Zheng, "An audio-based fault diagnosis method for quadrotors using convolutional neural network and transfer learning," in *2020 American Control Conference*. IEEE, 2020, pp. 1367–1372.

[59] L. Alzubaidi, J. Zhang, A. J. Humaidi, A. Al-Dujaili, Y. Duan, O. Al-Shamma, J. Santamaría, M. A. Fadhel, M. Al-Amidie, and L. Farhan, "Review of deep learning: Concepts, cnn architectures, challenges, applications, future directions," *Journal of Big Data*, vol. 8, no. 1, pp. 1–74, 2021.

[60] X. Liu, J. Yin, J. Liu, P. Ding, J. Liu, and H. Liub, "Trajectorycnn: a new spatio-temporal feature learning network for human motion prediction," *IEEE Transactions on Circuits and Systems for Video Technology*, 2020.

[61] X. Lei and Z. Sui, "Intelligent fault detection of high voltage line based on the faster r-cnn," *Measurement*, vol. 138, pp. 379–385, 2019.

[62] X. Liang, "Image-based post-disaster inspection of reinforced concrete bridge systems using deep learning with bayesian optimization," *Computer-Aided Civil and Infrastructure Engineering*, vol. 34, no. 5, pp. 415–430, 2019.

[63] F. Zhang, V. Bazarevsky, A. Vakunov, A. Tkachenka, G. Sung, C.-L. Chang, and M. Grundmann, "Mediapipe hands: On-device real-time hand tracking," *arXiv:2006.10214*, 2020.

BIOGRAPHY

Meng-Lun Lee received the B.S. degree in electrical engineering in 2007 from Chung Yuan Christian University, the M.S. degree in mechanical engineering in 2011 from National Chung Cheng University, and since 2019 he has been a Ph.D. candidate in the Department of Mechanical and Aerospace Engineering, University at Buffalo, NY, USA. His research interests include robotics, artificial intelligence, and vision-guided robotic systems with human-robot collaboration.

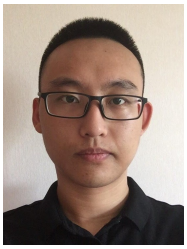

Wansong Liu received the B.S. degree in materials processing and controlling engineering in 2017 from the China University of Mining and Technology, Xuzhou, China, and the M.S. degree in mechanical and aerospace engineering in 2020 from the University at Buffalo, Buffalo, NY, USA, where he is currently working toward the Ph.D. degree in mechanical engineering. His research interests include planning, learning, and the control of robotic manipulators in collaboration with human.

Sara Behdad received the B.S. and M.S. degrees in Industrial Engineering from Tehran Polytechnic and her Ph.D. degree in Industrial and Enterprise Systems Engineering in 2013 from the University of Illinois at Urbana-Champaign, IL, USA. She is currently an Associate Professor at the Engineering School of Sustainable Infrastructure & Environment at the University of Florida, FL, USA. She has served as an associate editor for the ASME Journal of Mechanical Design and Journal of Manufacturing Science and Engineering. Her research interests include sustainable design, remanufacturing, and product lifecycle engineering.

Xiao Liang received the B.S. degree in 2010 from Hunan University, Changsha, China, and the M.S. and Ph.D. degrees from the University of California, Berkeley, CA, USA, in 2011 and 2016, respectively, all in civil engineering. In 2018, he joined the University at Buffalo, Buffalo, NY, USA where he is currently an Assistant Professor in the Department of Civil, Structural, and Environmental Engineering. His research interests include health monitoring and autonomous inspection of infrastructure systems, and robotics and automation, with applications to human-robot collaboration for future remanufacturing.

Minghui Zheng received B.S. degree in engineering mechanics in 2008 and M.S. degree in control science and engineering in 2011, both from Beihang University, China, and the Ph.D. degree in mechanical engineering from University of California, Berkeley, CA, USA, in 2017. She joined the University at Buffalo, Buffalo, NY, USA, in 2017, where she is currently an Assistant Professor of mechanical and aerospace engineering. Her research interests include learning, planning, and control of multiple robotic systems, such as collaborative manipulators for remanufacturing and drones for disaster resilience. She was the recipient of the NSF CAREER Award in 2021.